Smart ultrasound device for non-invasive real-time myocardial stiffness quantification of the human heart

Olivier Pedreira, Mafalda Correia, Simon Chatelin, Olivier Villemain, Guillaume Goudot, Stéphane Thiébaut, Gioia Bassan, Emmanuel Messas, Mickaël Tanter, Clément Papadacci, and Mathieu Pernot**

***Abstract*—Quantitative assessment of myocardial stiffness is crucial to understand and evaluate cardiac biomechanics and function. Despite the recent progresses of ultrasonic shear wave elastography, quantitative evaluation of myocardial stiffness still remains a challenge because of strong elastic anisotropy. In this paper we introduce a smart ultrasound approach for non-invasive real-time quantification of shear wave velocity (SWV) and elastic fractional anisotropy (FA) in locally transverse isotropic elastic medium such as the myocardium. The approach relies on a simultaneous multidirectional evaluation of the SWV without a prior knowledge of the fiber orientation. We demonstrated that it can quantify accurately SWV in the range of 1.5 to 6 m/s in transverse isotropic medium (FA<0.7) using numerical simulations. Experimental validation was performed on calibrated phantoms and anisotropic ex vivo tissues. A mean absolute error of 0.22 m/s was found when compared to gold standard measurements. Finally, in vivo feasibility of myocardial anisotropic stiffness assessment was evaluated in four healthy volunteers on the antero-septo basal segment and on anterior free wall of the right ventricle (RV) in end-diastole. A mean longitudinal SWV of 1.08 ± 0.20 m/s was measured on the RV wall and 1.74 ± 0.51 m/s on the septal wall with a good intra-volunteer reproducibility (± 0.18 m/s). This approach has the potential to become a clinical tool for the quantitative evaluation of myocardial stiffness and diastolic function.**

***Index Terms*—Acoustic Radiation Force, Clinical device, Myocardial Stiffness, Shear Wave Velocity**

Manuscript received May 27, 2021; accepted June 02, 2021;
This study was supported by the European Research Council under the Horizon 2020 Framework Program / ERC Grant Agreement n° 665113. This study was also supported by BPI FRANCE (PACIFIC project) and INSERM Transfert (COPOC project). We acknowledge the ART (Technological Research Accelerator) biomedical ultrasound program of INSERM.
O. Pedreira (pedreiraolivier@gmail.com), M. Correia (mafilipa.correia@gmail.com), S. Chatelin (simon.chatelin@gmail.com), O. Villemain (olivier.villemain@sickkids.ca), S. Thiébaut (stephanethiebaut@gmail.com), G. Bassan (gioia.bassan@gmail.com), M. Tanter (mickael.tanter@gmail.com), C. Papadacci (clement.papadacci@espci.fr), and M. Pernot (mathieu.pernot@espci.fr) are with Physics for Medicine Paris, INSERM U1273, ESPCI Paris, PSL University, CNRS 8063, Paris, France. *C. Papadacci and M. Pernot contributed equally to this study.
G. Goudot (guillaume.goudot@gmail.com) and E. Messas (emmanuel.messas@aphp.fr) are with Hôpital Européen Georges Pompidou, APHP, Vascular Medicine Department, Paris, France.

I. Introduction

Myocardial stiffness is a key biomechanical property of the cardiac mechanics and function. Myocardial stiffness alteration during contraction or relaxation is associated with heart failure, and consequently high risk of death [1]–[3] . Several methods have been proposed to assess myocardial stiffness using strain analysis [4] or the propagation of myocardial stretch [5], but up to date, despite the urgent clinical need, there is no non-invasive method available in clinical practice to assess myocardial stiffness quantitatively [6] .

The advent of ultrafast ultrasound imaging (UF) almost 20 years ago has enabled the observation of mechanical shear waves in soft tissues[7]. Based on the intrinsic relationship between shear wave velocity (SWV) and the shear modulus of soft tissues [8], UF imaging was rapidly envisioned as a tool for non-invasive and quantitative imaging of soft tissues elastic properties [9]. The combination of UF imaging and the remote generation of shear waves through the acoustic radiation force enabled the so-called shear wave elastography (SWE) modality which was successfully developed in the clinics for quantitative mapping of breast, liver and thyroid elasticity. Cardiac applications of SWE were also investigated extensively for the measurement of myocardial stiffness in the beating heart of preclinical models [10], [11]. With this approach, shear wave velocity could be measured at any moment of the cardiac cycle to assess stiffness variation [12], to provide a contractility index [13] or passive property estimations [14] respectively based on systolic and diastolic elastic properties. More recently, SWE was translated to human applications and the clinical proof of concept of myocardial SWE was demonstrated on healthy volunteer [15], [16] and hypertrophic cardiomyopathy patients [17].

Nevertheless, an important issue remained unsolved: the dependence of shear velocity with the local orientation of myocardial fibers. Indeed, muscular, tendinous and myocardial tissues are composed of fibers locally oriented along a principal direction (longitudinal direction). These soft solids can be assumed as locally transverse isotropic [18] materials in which a single shear modulus is no longer adequate to characterize the elastic properties[19]. As stiffness (and SWV) is higher along fibers than across them [20], [21], the complete stiffness tensor is required to characterize the elastic properties of anisotropic

tissues such as the myocardium. Moreover, fiber orientation in the myocardium follows a complex helical distribution of bundle which is patient dependent. Therefore, with 2D imaging, SWV is measured in an unknown direction with respect to the fiber orientation creating important variability on SWV evaluation and a certain ambiguity to what stiffness parameter is really measured.

A potential solution to solve this problem is the Elastic Tensor Imaging (ETI) approach [22] to retrieve the full wave propagation from several measurements performed at different angles using a mechanical rotation of the probe, but this setup was not applicable in real-time and thus not suitable for clinical use. More recently, ETI was implemented using 3D UF imaging with matrix probes which offered the possibility to track the transient shear wave in a single 3D acquisition [23], [24]. However, this approach relies on complex and costly hardware in terms of probes, wirings and electronics to drive thousands of independent piezoelectric elements, and cannot be applied in its current form to clinical applications.

In this work, we propose an innovative solution based on multidirectional SWV evaluation with a smart ultrasound approach to achieve real-time myocardial anisotropic stiffness quantification in human patients. The transducer was designed specifically for imaging fibrous tissues and to retrieve the SWV parameters in locally transverse isotropic medium. This device has the capacity to measure automatically the myocardium stiffness at a predetermined timing of the cardiac cycle and allows the automatic determination of the probe alignment with the myocardium fibers. Although the device design is simple and consists in only 8 transducer elements, it can achieve simultaneous anisotropic shear velocity estimation that would require normally a much more complex system such as matrix probes with thousands of elements.

The concept was validated using numerical simulations in the first part of the study. Then, the device was experimentally validated against gold standard in calibrated phantoms and ex vivo fibrous tissues. Finally, in vivo and transthoracic feasibility of end-diastolic myocardial stiffness evaluation was demonstrated in human volunteers. This approach has the potential to become a clinical tool for the quantitative evaluation of myocardial stiffness in diastole but also at any time of the cardiac cycle.

II. Materials and Methods

A. Shear Wave Velocity in transverse anisotropic medium

Let's consider a linear transverse isotropic elastic solid with a (y_0, x_0) isotropic plane (i.e. the plane normal to the fiber direction) and z_0 axis of symmetry (Figure 1). The fourth-rank stiffness tensor can be simplified by using the 2-index Voigt notation:

$$C = \begin{bmatrix} c_{11} & c_{11}-2c_{66} & c_{13} & 0 & 0 & 0 \\ c_{11}-2c_{66} & c_{11} & c_{13} & 0 & 0 & 0 \\ c_{13} & c_{13} & c_{33} & 0 & 0 & 0 \\ 0 & 0 & 0 & c_{44} & 0 & 0 \\ 0 & 0 & 0 & 0 & c_{44} & 0 \\ 0 & 0 & 0 & 0 & 0 & c_{66} \end{bmatrix} \quad (1)$$

where $c_{13} = \sqrt{c_{33}(c_{11}-c_{66})}$

The Christoffel equation was used to derive the velocity of mechanical waves that propagate in such solid. The group velocity of a shear wave polarized along x_1 and propagating in the (y_1, z_1) plane (probe coordinate system) can be expressed as follow[25]:

$$\rho v_r(\theta)^2 = \frac{C_{44}C_{66}}{C_{44}sin^2(\theta+\theta_0) + C_{66}cos^2(\theta+\theta_0)} \quad (2)$$

With $v_r(\theta)$ the group velocity, θ the angle defining the propagation direction and θ_0 the orientation of the fibers in the (y_1, z_1) probe coordinate system.

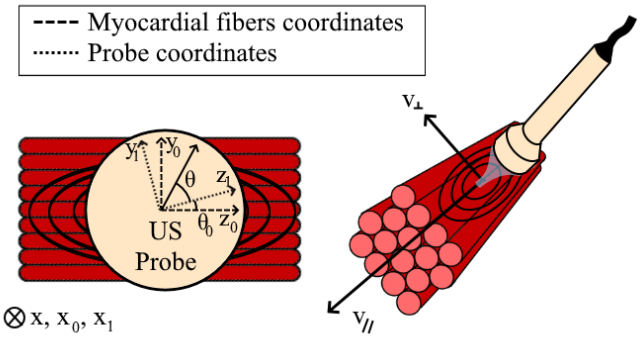

Fig. 1 Representation of fibers orientation in the probe coordinate system (y_1, z_1). Fibers are oriented along θ_0 . The SW is tracked along a direction θ. Representation of parallel SWV ($v_{\parallel}$) direction and perpendicular SWV ($v_{\perp}$) direction.

B. Deriving SWV using Elastic Tensor Imaging (ETI)

The concept of ETI was introduced by Lee et al.[22]. Shear wave propagation properties (c_{44}, c_{66}, θ_0) were retrieved from a limited number of shear wave velocity measurements (v_{rN}) estimated along different propagation directions (θ_N). Linearization of Eq.2 was performed:

$$\frac{1}{\rho {v_r}^2} = \frac{1}{2\,C_{44}C_{66}} \cdot \begin{pmatrix} C_{44}\left(1-\cos\left(2(\theta+\theta_0)\right)\right) \\ +\,C_{66}\left(1+\cos\left(2(\theta+\theta_0)\right)\right) \end{pmatrix} \quad (3)$$

Then

$$\frac{2}{\rho {v_r}^2} = \frac{C_{44}+C_{66}}{C_{44}C_{66}} + \frac{C_{66}-C_{44}}{C_{44}C_{66}}\cos(2\theta)\cos(2\theta_0) - \frac{C_{66}-C_{44}}{C_{44}C_{66}}\sin(2\theta)\sin(2\theta_0) \quad (4)$$

A change of variables is performed to simplify the notations:

$$\begin{bmatrix} X_1 \\ X_2 \\ X_3 \end{bmatrix} = \begin{bmatrix} (C_{44}+C_{66}) \,/\, C_{44}C_{66} \\ ((C_{66}-C_{44}) \,/\, C_{44}C_{66}) * \cos(2\theta) \\ ((C_{44}-C_{66}) \,/\, C_{44}C_{66}) * \sin(2\theta) \end{bmatrix} \quad (5)$$

We obtain a system of linear equations composed of the different measurements v_{rN} performed along different directions θ_N:

$$\begin{bmatrix} 2/\rho {v_{r1}}^2 \\ \vdots \\ 2/\rho {v_{rN}}^2 \end{bmatrix} = \begin{bmatrix} 1 & \cos(2\theta_1) & \sin(2\theta_1) \\ \vdots & \vdots & \vdots \\ 1 & \cos(2\theta_N) & \sin(2\theta_N) \end{bmatrix} . \begin{bmatrix} X_1 \\ X_2 \\ X_3 \end{bmatrix} = \phi . \begin{bmatrix} X_1 \\ X_2 \\ X_3 \end{bmatrix} \quad (6)$$

Inversion of the linear system can be performed with at least three independent measurements using the least-square method to provide an estimate of X_1, X_2, X_3

$$\begin{bmatrix} X_1 \\ X_2 \\ X_3 \end{bmatrix} = (\phi^T.\phi)^{-1}.\phi^T.\begin{bmatrix} 2/\rho {v_{r1}}^2 \\ \vdots \\ 2/\rho {v_{rN}}^2 \end{bmatrix} \quad (7)$$

Finally, we obtain the three unknown parameters as follow:

$$\theta_0 = \frac{1}{2}\text{atan}\left(\frac{X_3}{X_2}\right)$$

$$C_{66} = \frac{1}{2\left(X_1 - \frac{X_2}{\cos(2\theta_0)}\right)} \text{ and } C_{44} = \frac{1}{2\left(X_1 + \frac{X_2}{\cos(2\theta_0)}\right)} \quad (8)$$

Consequently, the shear modulus along and across the fibers and the fiber direction can be derived using at least 3 arbitrary measurements of the wave propagation in independent directions. Herein, we designed a dedicated probe based on this principle. In the following, the medium properties will be expressed in term of shear velocity along (parallel $v_\parallel$) and across (perpendicular $v_\perp$) the fibers using the relationship:

$$v_\parallel = \sqrt{C_{66}/\rho}, \qquad v_\perp = \sqrt{C_{44}/\rho} \ , \quad (9)$$

We will also quantify the Fractional Anisotropy (FA) parameter, between 0 to 1 (Isotropic to strongly anisotropic) using the following expression:

$$FA = \sqrt{2}\,\frac{\sqrt{(v_\perp - v_m)^2 + (v_\parallel - v_m)^2}}{\sqrt{{v_\perp}^2 + {v_\parallel}^2}} \quad (10)$$

With v_m the mean velocity of perpendicular ($v_\perp$) and parallel ($v_\parallel$) SWV.

C. Transducer Design

We designed an ultrasonic transducer composed of a small number of individual piezoelectric elements to generate remotely a shear wave using the acoustic radiation force and to detect the tridimensional shear wave propagation along different directions.

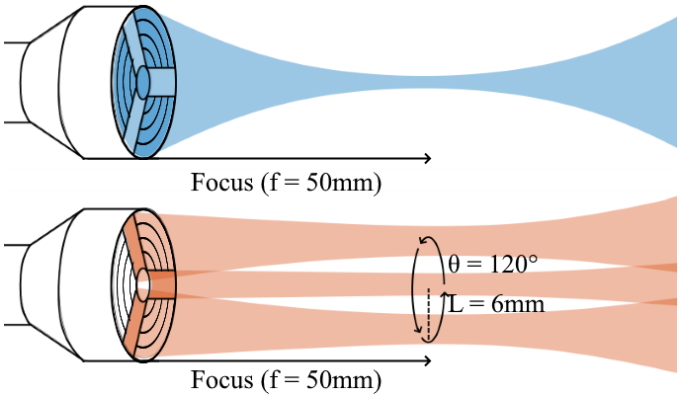

Fig. 2. Design of the ultrasound probe for multidirectional SWV assessment. In blue, representation of the beam generated by the five annular elements focused at f=50mm. In orange, representation of the beams generated by the three lateral elements. The lateral element centers are set radially with a 120° angular spacing.

The transducer was designed with five portions of concentric annular elements and three lateral elements (See figure 2). This transducer was manufactured by Imasonic. The annular elements are designed to 1) focus an ultrasound wave and generate the acoustic radiation force at the desired depth and 2) perform a real-time M-mode imaging for the positioning of the device. The probe is geometrically focused at 90mm. Electronical focusing was achieved using the annular elements to adjust the focus at the desired depth between 20mm and 90mm. Lateral elements are set radially with a 120° angular spacing and are designed to estimate local tissue motion in dedicated locations surrounding the pushing location. The angular spacing between the lateral elements was set as large as possible, to minimize the estimation error on the reconstructed shear velocity profile. The design of the probe is shown on Fig. 2. The two operation modes are presented: the focused mode for M-mode imaging and push generation and the pulse echo detection mode using the lateral elements.

D. Numerical Simulation

In order to validate and understand the limitations of this approach, we performed in this section a four-steps numerical simulation that include both acoustic and elastic wave propagations:

1. Acoustic radiation force field was computed in 3D with the ultrasound simulation software Field II.
2. Shear wave propagation generated by the acoustic radiation force in a transverse isotropic medium was computed using an anisotropic Green's function formalism.
3. Acoustic simulation was performed with Field II to compute the pulse echo signals received by the lateral elements during the propagation of the shear wave in a random scatterer distribution. The scatterer motion was set accordingly to the shear wave displacement field computed in step 2.
4. Axial tissue velocity was estimated from the pulse echo signals. Time of flight was estimated for each of the 3 lateral directions. Eq.7 was used to derive the medium properties (shear velocity along and across the fibers, fiber direction).

1) Simulation of the acoustic radiation force field

Field II ultrasound simulation software [26], [27] was used to compute the pressure field emitted by the concentric annular elements of the transducer over a 3D volume. The simulation parameters are detailed in Table 1. The acoustic radiation force field (F) was obtained as $F = (2\alpha I)/c$ where α is the absorption coefficient and I the acoustic intensity computed as $I = P^2/(2Z)$ with P is the pressure amplitude and Z the acoustic impedance.

TABLE I
FIELD II - SIMULATION PARAMETERS (ACOUSTIC RADIATION FORCE)

Transducer discretization pitch	0.25 mm^2
Attenuation	150 dB/m
Transducer Center Frequency	2.5 MHz
Sampling Frequency	250 MHz
Transmit Duration	300 µs
Focus Depth	50 mm
Acoustic Impedance	1.48 x 10^6 $kg.m^{-1}.s^{-2}$
Size of the simulation grid	
X Direction	-20 : 0.1 : 20 mm
Y Direction	-20 : 0.1 : 20 mm
Z Direction	0 : 0.1 : 150 mm

2) Simulation of the shear wave propagation

The shear wave propagation was computed using a transverse isotropic viscoelastic Green's function formalism [28] . In brief, this Green's function offers an analytical description of elastic wave propagation from a point source in a transverse isotropic material. The simulation assumed a non-viscous medium. Further details on the numerical method and implementation in soft tissues can be found in [18]. The acoustic radiation force 3D field computed in step 1 was used as the shear source term of the simulation. The displacement field **D(x,y,z,t)** created by the shear wave was computed at each temporal sampling point. We investigated a wide range of elastic parameters to assess the accuracy and the limitations of the method by varying the parallel and perpendicular shear velocities and the fractional anisotropy

Two sets of parameters were used. At first, we investigated the maximal shear wave velocity that can be measured with the system by increasing the SWV, $v_{\parallel}$ from 1.50 m/s to 6.00 m/s and $v_{\perp}$ while the FA was kept constant. Secondly, we investigated the maximal FA that can be measured with our system by increasing $v_{\parallel}$ from 1.50 m/s to 5.00 m/s while $v_{\perp}$ was maintained constant (1.50 m/s) resulting in an FA increase from 0.20 to 0.78. The datasets values were chosen in the range of pathological and healthy tissues from previous studies.

The parameters of the simulation are summarized in Table II. The compression velocity ($\boldsymbol{c_P}$), was considered homogenous on the entire sample. The medium density ($\boldsymbol{\rho}$) was chosen to mimic the human tissues density and the sampling frequency ($\boldsymbol{Fs}$) was fixed to be similar with the probe lateral elements framerate.

TABLE II
GREEN SIMULATION PARAMETERS

Compression Velocity	$\boldsymbol{c_P}$	1500 m/s
Medium Density	$\boldsymbol{\rho}$	1038 g/cm^3
Sampling Frequency	$\boldsymbol{F_s}$	10 000 Hz
- 1st Dataset		
Perpendicular SWV	$\boldsymbol{v_{\perp}}$	[1.50-2.00-2.50-3.00-3.50-4.00-4.50] m/s
Parallel SWV	$\boldsymbol{v_{\parallel}}$	[2.00-2.67-3.33-4.00-4.67-5.33-6.00] m/s
- 2nd Dataset		
Perpendicular SWV	$\boldsymbol{v_{\perp}}$	[1.50-1.50-1.50-1.50-1.50-1.50-1.50] m/s
Parallel SWV	$\boldsymbol{v_{\parallel}}$	[2.00-2.50-3.00-3.50-4.00-4.50-5.00] m/s

3) Pulse-echo simulation of the shear wave detection

Pulse echo signals received by each of the 3 lateral elements were simulated using Field II. A collection of 20 000 randomly distributed scatterers (80 scatterers / mm^3) was used to generate the backscattered signal. The scatterers were assumed to be spherical isotropic point sources. The displacement field $\boldsymbol{D(x,y,z,t)}$ obtained in the previous step was applied on scatterer positions $\boldsymbol{S_t = S_0 + D(x,y,z,t)}$. A pulse echo simulation was performed for each distribution $\boldsymbol{S_t}$ of the scatterers at high repetition rate (10 000Hz). The set of radio-frequency signals was then generated for each lateral element. A random noise was added to RF signal with a 5% amplitude the resulting SNR (Signal to Noise Ratio) was 27.3 dB.

4) Post-processing steps and shear velocity quantification

Axial tissue velocities were obtained at each depth and for each lateral element from successive RF signals using the Kasai estimator [29]. After low pass filtering (Butterworth filter, cut frequency 500Hz, order 5), the time of flight of the shear wave propagation was determined as the difference between the end of the pushing time and the time to peak velocity estimated at the lateral position under the assumption of purely elastic or mildly dispersive media [30], [31] for each of the lateral element. The three parameters θ, C_{66} and C_{44} are derived from equation (7). Using eq.9, shear velocities along and across the fibers and the fiber directions were assessed. The result was displayed as an elliptical profile of the shear velocity. It should be noted that the velocity profile of equation (2) is not a pure ellipse [32] however for the sake of simplicity we will refer in the following as an "elliptic profile". A motion correction was applied to remove the overall motion of the tissue by subtracting the mean displacement within the duration of the UF acquisition. This step was necessary only for in vivo acquisitions on human heart.

E. Experimental validation

The probe presented in Section II.C was manufactured and connected to a research ultrasonic device (Vantage 64, Verasonics, Seattle, USA). A user interface software was developed to position the probe and trigger the acquisitions.

1) M-Mode imaging

Due to elements disposition M-Mode imaging was performed for positioning by using the concentric annular elements. Ultrasonic beams (central frequency of 2.5 MHz) were focused at a depth of 50 mm with a PRF of 480 Hz using a pulse inversion scheme and harmonic imaging implemented to remove the clutter noise and increase the contrast of the images [33]. Backscattered signals were received, filtered and beamformed using a conventional delay and sum algorithm. A dedicated software was developed to provide a real time M-Mode imaging using the annular elements with an effective framerate of 200 Hz to allow the positioning.

2) SWE sequence

To generate the SW a US burst at the frequency of 2.5 MHz was focused during 350µs. The push was immediately followed by UF imaging acquisition using each of the three lateral elements simultaneously. Pulse echo imaging was performed at high framerate (10 000Hz) during 15ms for tissue velocity estimation. The signals received by the three laterals elements were then post processed. The post-processing method detailed in D.4 for synthetic data was applied to the experimental RF signals.

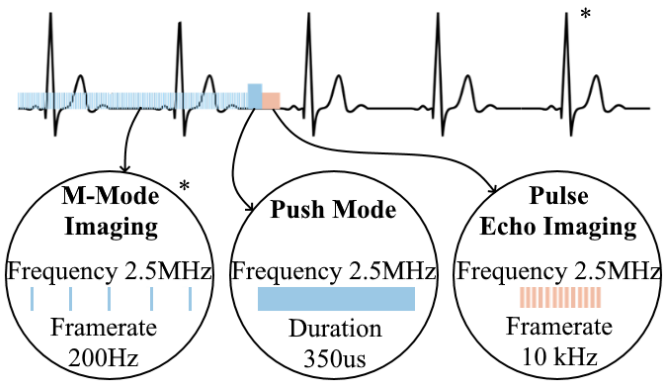

Fig. 3. Representation of the sequence for *in-vivo* stiffness evaluation. The device allows a real-time M-Mode imaging to correctly position the probe. Shear wave generation is performed in diastole using ECG trigger. Right after the push, the system switch to Pulse Echo Imaging using the lateral elements to track the shear wave. *ECG trigger and M-Mode Imaging are only used for in-vivo cardiac measurements.

3) Acoustic calibrations

The pressure field emitted by the annular and lateral elements were calibrated using a bilaminar PVDF membrane hydrophone (Acertara 805). The hydrophone was mounted on a 3-axis motorized Acertara measurement tank in order to scan the pressure field in the entire volume. The Mechanical Index (MI) and ISPTA were measured for the push beam and the lateral elements beams. The MI was 1.33, TI was 0.87 and the ISPTA was 364 mW/cm^2. These verifications were done to ensure the safety of the sequence.

4) In Vitro Isotropic phantoms

Validation was performed on four isotropic calibrated phantoms (CIRS, Zerdine®, model 039) with SWV values of 0.92m/s – 1.49m/s – 2.58m/s and 3.49 m/s provided by the manufacturer. For each phantom, 100 measurements at different locations were performed to evaluate the measurement variability.

5) Ex-Vivo tissue samples

Three ex-vivo samples of anisotropic skeletal muscle and left ventricular tissue were used. The first model was a chicken breast, the second was an ex-vivo bovine muscle sample and the last model was a porcine left ventricular sample. The samples were placed in saline water and were imaged at a distance of Z = 50mm. A validation against SWV measurements from Aixplorer® scanner (Supersonic Imagine, France), gold standard for SWE, was performed for the skeletal muscle samples using a linear conventional probe SL10-2 attached to a motorized rotation device.

6) Human acquisitions

Transthoracic acquisitions were performed on four healthy volunteers by a trained cardiologist. The study was approved by the french ethical committee (comité de protection des personnes) and each volunteer gave informed consent. The volunteers were positioned in left lateral decubitus position. The probe was positioned in parasternal view and aligned on the antero septo basal segment using M-Mode imaging.

The acquisition was triggered in mid diastole using an external clinical ECG device (Accusync). The ECG signal was converted in a numerical signal and continuously recorded using an external microcontroller device. The R wave was detected to trig the system at a specific time. Trigger time was adjusted manually by the operator on the user interface. The system trigger and ECG signals were also recorded to ensure the right acquisition timing in post-processing.

The sequence is represented in Figure 3. Five acquisitions were performed by the same operator on each volunteer at different heart beat to investigate the intra-volunteer reproducibility. Each acquisition corresponded to a single multidirectional SWV estimation using one push. To evaluate RV and septal SWV the operator determined the location of the walls based on the M-Mode imaging. Post-processing time was less than a second.

III. Results

A. Numerical validation

The acoustic intensity map (spatial peak pulse average intensity map ISPPA) computed by Field II is shown on Figure 4. The maximum intensity was found at a depth of 57.5 mm. The -6dB focal spot dimensions was 61.1mm in the axial direction and 1.4 mm in the radial direction.

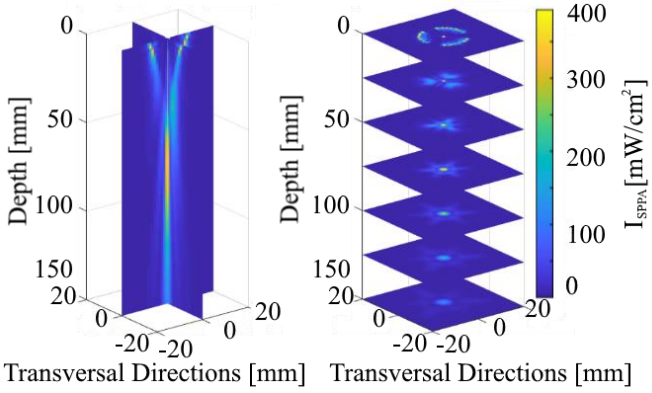

Fig. 4. Numerical simulation of the acoustic intensity focalization field used to generate the radiation force (Field II software).

The shear wave generated by the acoustic radiation force term was then computed using the Green's function formalism in transverse isotropic medium. An example of the resulting elliptic displacement wave front is shown on Figure 5.A at t=3.5ms for parallel and perpendicular shear wave speeds set respectively to 2.00 m/s and 1.50 m/s. Pulse-echo imaging was then simulated for each lateral element. The central positions of lateral elements are superimposed on figure 5.A. After motion estimation, the temporal tissue velocity profile was obtained for the three lateral elements (Figure 5.B).

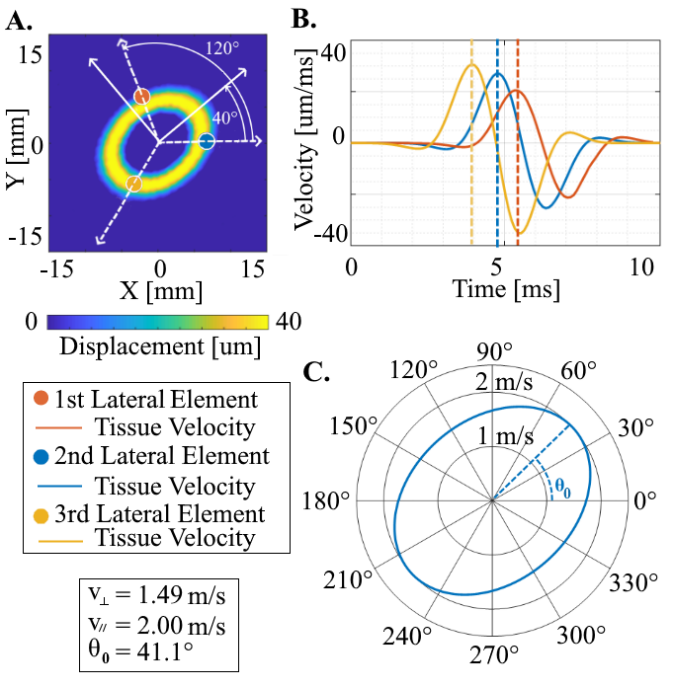

Fig. 5. **A.** Displacement field of the shear wave propagation at a depth of Z = 50mm and t = 3.5ms. The markers show the central position of the lateral elements. **B.** Tissue velocity estimated by the three lateral elements used to evaluate the shear wave speed. **C.** Medium properties were derived and the elliptic profile of the shear velocity was reconstructed. Time of flight estimation was performed to assess the group velocity in the three directions. Finally, after inversion of Eq. 6, the shear modulus in parallel and perpendicular directions as well as the fiber direction were retrieved. The shear velocity profile shown in Figure 5.C was reconstructed from Eq.2. In this example, we obtained $\upsilon_{\parallel}$ = 2.00 m/s, $\upsilon_{\perp}$ = 1.49 m/s and θ= 41.1° which was in good agreement with the simulation parameters ($\upsilon_{\parallel}$ = 2.00 m/s, $\upsilon_{\perp}$ = 1.50 m/s and θ= 40.0°).

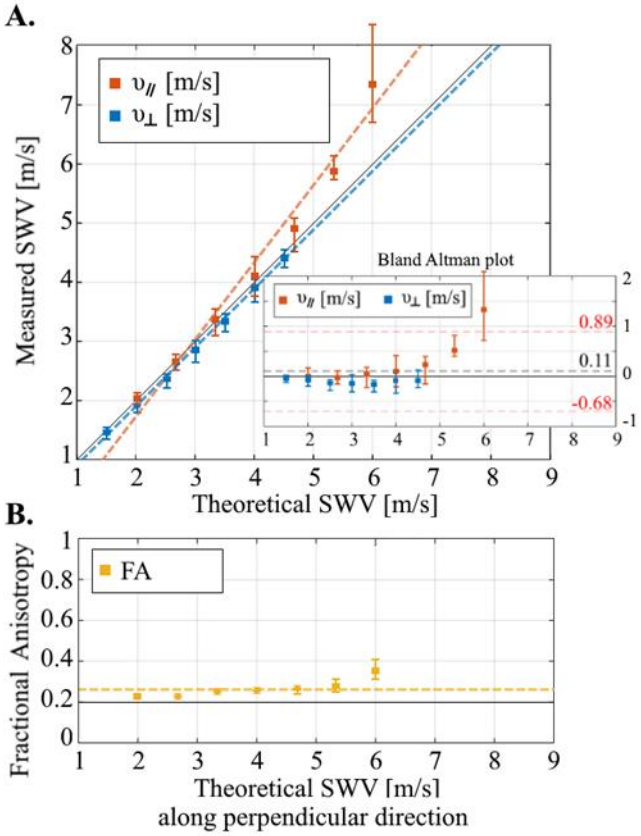

Fig. 6. Estimation of SWV (fixed FA). **A.** Estimated Shear Wave Velocity along parallel ($\upsilon_{\parallel}$) and perpendicular ($\upsilon_{\perp}$) direction and Bland Altman plot between measured and Theoretical SWV, mean value 0.11m/s, mean+0.96SD = 0.89m/s, mean-0.96SD = -0.68m/s **B.** Estimated fractional anisotropy, mean 0.28 mean absolute error 0.078 (26%)

Results of the SWV computed by the simulation are presented on figure 6 and 7. Figure 6 presents the results for a fixed FA model. SWV estimates were in good agreement with the simulation parameters. The mean difference between the estimates and the theoretical perpendicular and parallel SWV found was respectively 0.11 m/s (3.6%) and 0.33 m/s (6.1%). The FA estimates were also close to the theoretical values with a mean absolute error of 0.078 (26%).Figure 7 show the results for the increased FA model. The mean difference between the estimates and the theoretical perpendicular and parallel SWV found was respectively 0.02 m/s (1.6%) and 0.36 m/s (8.0%). The FA estimates were also close to the theoretical values with a mean absolute error of 0.065 (15%). Perpendicular velocity was fixed to 1.5 m/s and the estimate showed a mean absolute difference of 0.023 m/s (15%) and a standard deviation of 0.009 m/s.

It should be noted that in both results, the estimation was particularly accurate for SWV below 5.0 m/s and becomes less accurate at higher velocity.

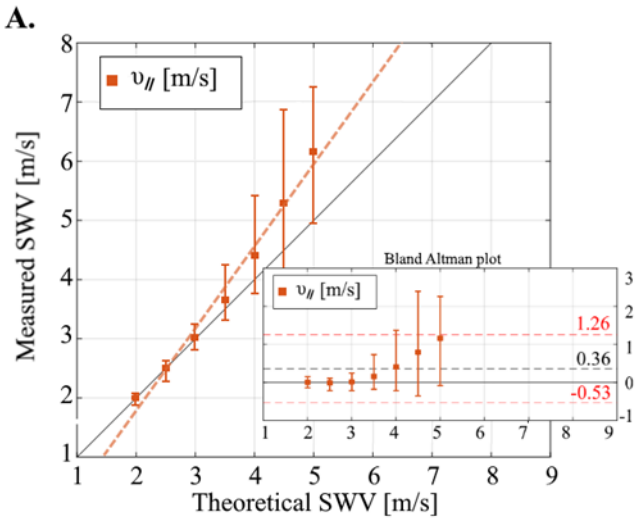

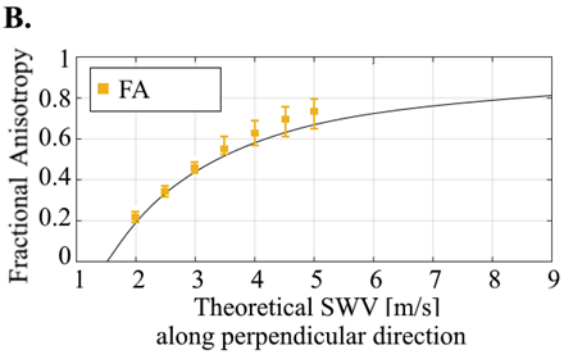

Fig. 7. Estimation of SWV (varying FA). **A**. Estimated Shear Wave Velocity along parallel ($v_{\parallel}$), perpendicular ($v_{\perp}$) direction. $v_{\perp}$ was fixed to 1.5 m/s and Bland Altman plot between measured and Theoretical SWV, mean value 0.36m/s, mean+0.96SD = 1.26 m/s, mean-0.96SD = -0.53 m/s **B.** Comparison of Fractional anisotropy estimates and theoretical values mean absolute error 0.065 (15%).

B. Experimental validation

1) Isotropic Phantoms

Shear wave velocity was evaluated in different calibrated phantoms. Agreement with the shear wave values provided by the manufacturer were found to be good (Figure 8) with a mean absolute error of 0.04 m/s. On the figure 8 we show the mean value between orthogonal and paralleled SWV and the computed FA. The FA mean value was 0.08 close to zero which is expected in isotropic medium.

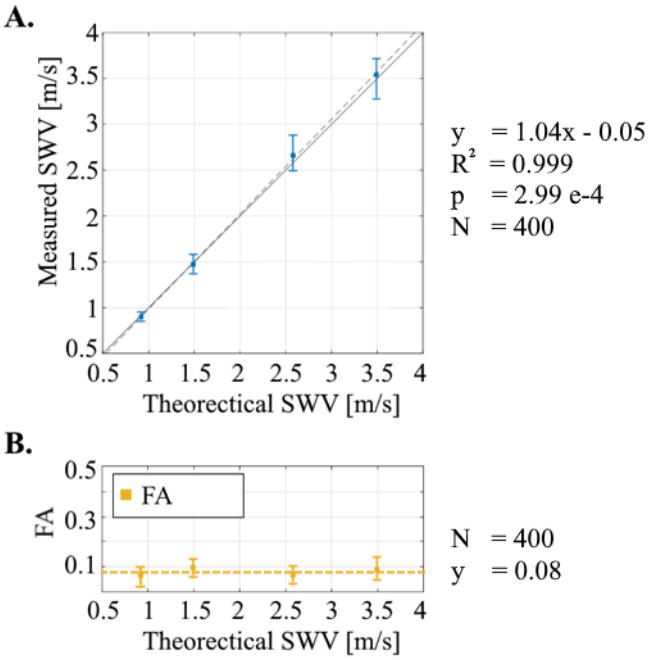

Fig. 8. Comparison of theoretical and measured shear wave velocity on 4 calibrated elastography phantoms. Measurement was repeated 100 times for each phantom.

2) Ex Vivo samples

The system was validated on two ex vivo skeletal muscle samples using a 2D commercial shear wave elastography system (Aixplorer®) as explained in the method section.

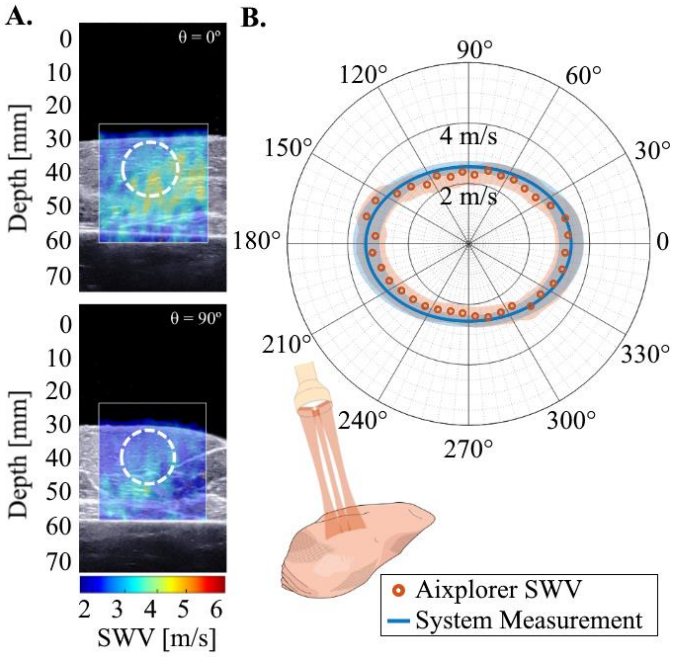

Fig. 9. In vitro validation in chicken breast. **A.** Shear modulus maps obtained using the Aixplorer® ultrafast scanner. The probe was rotated each 10º to provide a stiffness estimate in each direction. Maps along (0º) and across (90º) the tissue fibers are shown. **B.** SWV profile reconstructed from a single acquisition using our smart sensor in solid line superimposed onto the Aixplorer® measurements.

Figure 9 shows the comparison of Aixplorer® ultrafast scanner measurements (with rotation of the probe) and the shear velocity profile reconstructed with our system (without probe rotation) on chicken breast. $v_{\perp}$ = 2.3 m/s and $v_{\parallel}$ = 3.5 m/s for Aixplorer device versus $v_{\perp}$ = 2.57 m/s and $v_{\parallel}$ = 3.39 m/s for our device were found. It shows a good agreement of the measurements. A mean absolute error of 0.24 m/s was found.

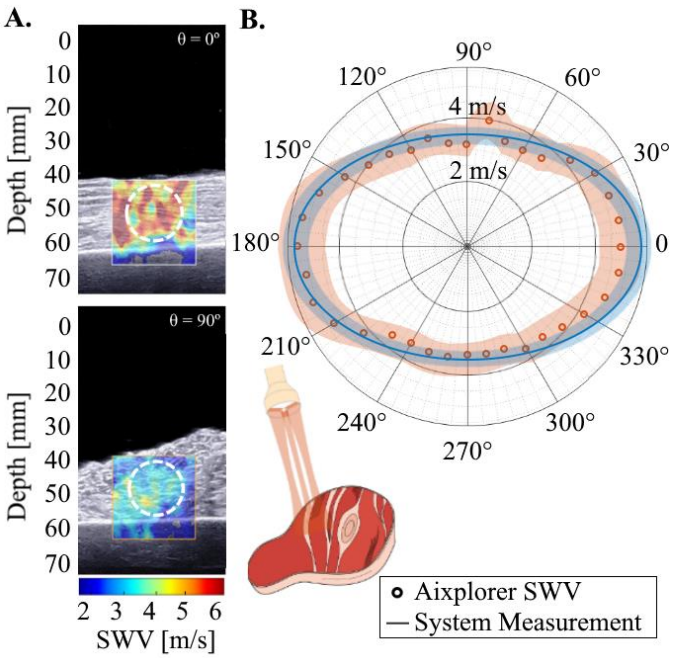

Fig. 10. In vitro validation in bovine muscle. **A.** Shear modulus maps obtained using the Aixplorer®. The probe was rotated each 10º to provide a stiffness estimate in each direction. Results along (0º) and across (90º) the tissue fibers are shown. **B.** SWV profile reconstructed from a single acquisition from the smart sensor in solid line superimposed onto the Aixplorer® measurements each 10º.

Figure 10 shows the same comparison on bovine skeletal muscle. A good agreement was also found, the mean absolute error was 0.20 m/s which corresponded to a relative error of 4.88%. With the Aixplorer, we measured: $v_{\perp}$ = 3.2 m/s and $v_{\parallel}$ = 5.3 m/s. With the smart device, we measured: $v_{\perp}$ = 3.14 m/s and $v_{\parallel}$ = 5.10 m/s. Summary of the results is presented on table IV.

Table IV shows the transverse and longitudinal SWV estimates for the two measurements. The SD values were computed with 5 measurements with the proposed system. For Aixplorer the SD is computed on the ROI represented on the figure 9 and 10.

TABLE IV
EX VIVO RESULTS

Chicken Breast Tissue			
Aixplorer® System		**Smart ultrasound device**	
$v_{\perp}$	2.35 +/- 0.3 m/s	$v_{\perp}$	2.57 +/- 0.17 m/s
$v_{\parallel}$	3.25 +/- 0.5 m/s	$v_{\parallel}$	3.39 +/- 0.33 m/s
FA	0.22	**FA**	0.19 +/- 0.09
Beef Skeletal Muscle			
Aixplorer® System		**Smart ultrasound device**	
$v_{\perp}$	3.30 +/- 0.5 m/s	$v_{\perp}$	3.52 +/- 0.19m/s
$v_{\parallel}$	5.05 +/- 0.8 m/s	$v_{\parallel}$	5.56 +/- 0.10m/s
FA	0.29	**FA**	0.31 +/- 0.02

Finally, ex vivo experiment was performed in a fresh porcine left ventricular sample. Because the fiber direction varies rapidly across the wall, it was not possible to compare directly with Aixplorer® measurements.

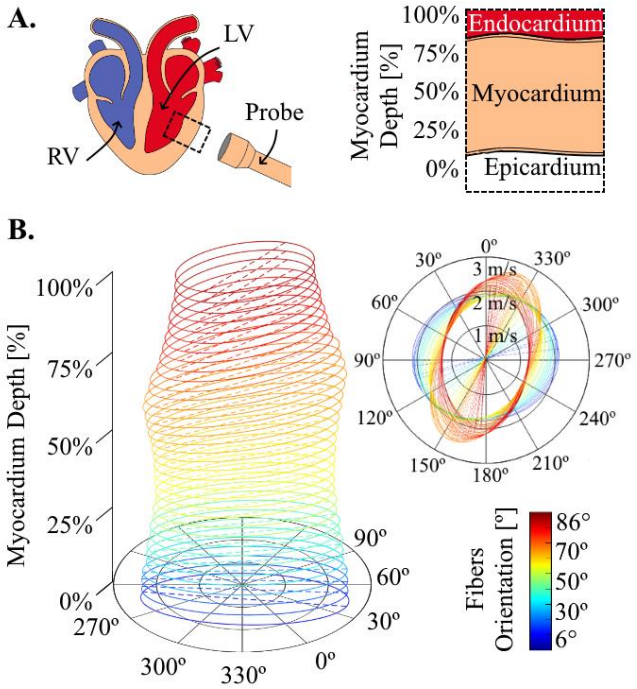

Fig. 11. Transmural variation of fibers orientation in ex vivo porcine samples. **A.** Schematic view of acquisition process, the US probe is aligned with the LV wall. **B.** Elliptic SWV profiles showing the fiber orientation as a function of transmural depth.

Nevertheless, the variation of the shear velocity profiles with the smart ultrasound approach was analyzed across the wall. Figure 11 shows the reconstructed elliptic shear velocity profiles from epicardium to endocardium resulting in an approximately 90° rotation in longitudinal direction of the fibers disposition in explanted ex vivo porcine LV measurement.

C. In Vivo feasibility

Finally, myocardial SWV was assessed in the heart of four human volunteers. Figure 12 shows an example of measurement. Real-time M-Mode positioning allowed visualization of RV and septal walls (Figure 12 A). Real-time ECG analysis allowed triggering acquisition in mid-diastole. Tissue velocity profiles in the RV and the septum of one volunteer is displayed on figure 12 B. The two SWV profiles were reconstructed (Figure 12 C) and transverse/parallel velocities were estimated. RV was found softer than the septum.

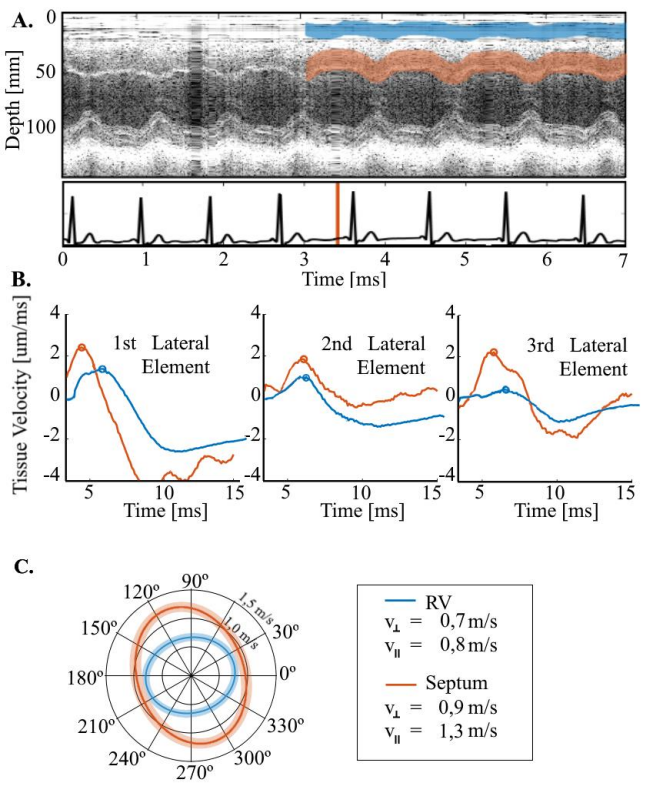

Fig. 12. In vivo Myocardial SWV estimation on a volunteer. **A.** M-Mode and ECG controller, the Right Ventricle (RV) wall is delineated in blue on the M-Mode and the septal segment in orange. **B.** RV and Septum walls velocity estimated from the pulse echo signals. Time of flight, here represented with circle markers, was estimated for each of the 3 lateral directions. **C.** The two SWV profiles and the transverse/parallel velocities are estimated from one single acquisition.

Individual and average results are presented on Table V. The average parallel SWV was 1.08m/s on the RV and 1.74 m/s on the septum. The intra patient reproducibility was +/-0.21 m/s along the fibers, +/- 0.15 across the fibers and +/-0.10 for the FA.

TABLE V
HEALTHY VOLUNTEERS MS

Volunteer		RV		Septum
1	$v_{\parallel}$	1.08 +/- 0.08 m/s	$v_{\parallel}$	2.44 +/- 0.22 m/s
	$v_{\perp}$	0.64 +/- 0.17 m/s	$v_{\perp}$	1.82 +/- 0.08 m/s
	FA	0.35 +/- 0.17	FA	0.20 +/- 0.04
2	$v_{\parallel}$	1.06 +/- 0.17 m/s	$v_{\parallel}$	1.68 +/- 0.26 m/s
	$v_{\perp}$	0.68 +/- 0.15 m/s	$v_{\perp}$	1.34 +/- 0.29 m/s
	FA	0.31 +/- 0.06	FA	0.22 +/- 0.07
3	$v_{\parallel}$	0.94 +/- 0.25 m/s	$v_{\parallel}$	1.20 +/- 0.20 m/s
	$v_{\perp}$	0.66 +/- 0.09 m/s	$v_{\perp}$	0.86 +/- 0.11 m/s
	FA	0.22 +/- 0.14	FA	0.22 +/- 0.14
4	$v_{\parallel}$	1.24 +/- 0.20 m/s	$v_{\parallel}$	1.64 +/- 0.15 m/s
	$v_{\perp}$	0.62 +/- 0.08 m/s	$v_{\perp}$	1.10 +/- 0.12 m/s
	FA	0.44 +/- 0.04	FA	0.27 +/- 0.08
Average				
	$v_{\parallel}$	1.08 +/- 0.20 m/s	$v_{\parallel}$	1.74 +/- 0.51 m/s
	$v_{\perp}$	0.65 +/- 0.12 m/s	$v_{\perp}$	1.28 +/- 0.48 m/s
	FA	0.33+/- 0.11	FA	0.23 +/- 0.09

The results are consistent with the values reported by previous studies.[17]

IV. DISCUSSION

In this study, we introduced a novel approach for quantitative assessment of myocardial stiffness. A smart ultrasound transducer was designed to achieve shear wave elastography in locally transverse isotropic soft medium. The approach was validated using numerical simulations as well as experiments in calibrated phantoms and biological samples. We demonstrated that this method is effective for assessing quantitatively the elastic properties of locally transverse isotropic soft tissues such as skeletal muscles and the myocardium without prior knowledge of the fiber orientation. Finally, we investigated the transthoracic feasibility on the heart of 4 human volunteers and showed that this approach was feasible and reproducible with an intra-patient variability of +/- 0.18 m/s. For comparison purposes, the SWV differences between control and hypertrophic cardiomyopathy patients were reported to be larger than 2 m/s on average thus one order of magnitude larger than the measurement variability [17].

This approach was developed to provide a clinical solution to the problem of angular dependence of shear velocity estimates with respect to myocardial fiber orientations. Previous studies of 2D myocardial SWE have proposed to perform shear wave velocity estimation along standardized anatomical views. For example, Villemain et al observed in pediatric and adult patients that the shear velocities in short axis view were significantly higher than in long axis view. Assuming that fibers were mainly oriented along the circumferential direction (i.e in short axis view), the FA was estimated to 0.24 ± 0.07 in adults and of 0.14 ±0.06 in children [17]. However, such an assumption does not hold on all patients, particularly those with fiber disarray, and generally speaking, it is difficult to assume the actual fiber orientation in human patients during echocardiography exam. Therefore, when applying 2D SWE imaging, the shear velocity is estimated in an unknown direction with respect to the fiber orientation. The discrepancy between parallel and transverse velocity may induce high variability among patient measurements and creates a certain ambiguity of which stiffness is really measured (along/across the fibers).

This work is the first in vivo assessment to our knowledge of simultaneous shear wave measurements in anisotropic medium. Other approaches for myocardial stiffness evaluation have relied on mechanical waves induced by physiological events such as valve closures (mitral or aortic valves [34]), blood pressure waves (atrial kick [35], [36]) or even by contraction propagation (electromechanical coupling [37]). Methods based on natural shear waves were shown to be feasible in vivo [34] and were recently applied to amyloidosis patients [38] with promising results. However, these approaches do not solve the problem of tissue anisotropy. Moreover, relying on natural shear waves has additional limitations: the generation of natural waves in the myocardium is a complex tri-dimensional phenomenon and is challenging to assess using 2D imaging [39], the wavelength of these natural waves is very large ~10cm which makes the wave velocity strongly dependent on myocardial anatomy and wall thickness. Moreover, the shear wave source is uncontrolled in terms of location, wavelength, amplitude and timing during the cardiac cycle [39]. 3D UF imaging approaches have been proposed [40]–[42] to image the

tri-dimensional wave propagation but in these studies the quantification of the velocity remains challenging. Moreover, none of these approaches could assess the elastic anisotropy of the myocardium.

In contrast, our approach is based on a well-controlled source location and timing using the acoustic radiation force. Thanks to the sharp shear source generated at a well-defined location in the myocardium, the resulting velocity profile can be quantified accurately in several directions simultaneously. We therefore achieved a 3D segmental estimation using a simple transducer design without the complexity of a full 3D UF imaging device. This design offers reliable and robust shear velocity estimate.

We designed intentionally a low complexity 8-element ultrasound device in order to ease as much as possible the clinical translational and dissemination. The system presented in this study could be entirely controlled by electronics with a lower complexity that high channel count used in 2D or 3D UF imaging.

This new approach could have several important applications in cardiology. Non-invasive stiffness assessment of the myocardium could become a major biomarker of diastolic dysfunction which remains difficult to quantify accurately with current clinical imaging tools. Myocardial stiffness could be applied to the diagnostic of heart failure with preserved ejection fraction, cardiomyopathies or cardiac amyloidosis, all of which remain difficult to diagnose. Non-invasive myocardial stiffness assessment could be also important for the diagnosis and prognosis of heart transplant recipient as proposed by Petrescu et al.[43]

We're confident that the probe design will be adapted to the majority of human anatomy. Using parasternal view will almost systematically allow at least RV measurement. The focal distance fixed with probe design and electronic can be adjustable by a few centimeters, nevertheless for large depth uses in obese patients, the probe could be adapted. It is also conceivable to measure stiffness in others anisotropic structures such as other fibrous tissues, heart valves or vessels as aorta but it may require some adaptations of the probe.

Nevertheless, our approach remains limited to the stiffness assessment of a limited number of myocardial segments and should be envisioned mostly for the diagnostic of diffuse or global heart impairments. We also assume the hypothesis of a homogenous tissue at the centimeter scale. Myocardial segments of about a centimeter in the right ventricular free wall and the septal wall can be assessed from the parasternal view as shown in this study whereas the septal wall and apical segment could be reached from the apical view. The left ventricular posterior wall, however, was not accessible because of the depth limitation of the current transducer. The epicardial to endocardial stiffness variation could also be an interesting parameter. In this study, however, we limited the shear velocity estimation at the mid-wall level on each volunteer. A more refined analysis could be performed on thick walls to investigate the transmural variation. Low ultrasound SNR could have an impact on velocity estimation, and our approach may be limited in obese or non-echogenic patients. The probe design and center frequency could be adapted to overcome this limitation.

In this study, we limited the acquisition of the myocardial stiffness on the human volunteer to the mid-diastolic phase. However, the acquisition can be performed at any time of the cardiac cycle for real time evaluation of myocardial elastic properties. SWV variation over the entire cardiac cycle could provide new insight of the cardiac function. Limitations of the study include the assumption of a purely elastic anisotropic material in Eq.2. The shear wave propagation model could be complexified in further study in order to include the viscosity properties. The lack of analytical solutions may however complicate the derivation of the visco-elastic properties.

A limitation of the approach is the need to estimate simultaneously three times of flight to achieve the inversion. For any reason, if one of the three estimates are missing, the inversion cannot be computed. We also observed that variability of the three measurement have a direct impact on ellipse shape resulting. Estimation of FA was however more sensitive to errors than parallel and perpendicular velocities. A large number of acquisitions can be performed to minimize this risk. Another potential solution would be to add several lateral elements in additional directions. It would allow to do measurement even if one element is missing but it would require to revise the transducer geometry. The inversion of the Eq.8 could be affected by low ultrasound signal to noise ratio (SNR). The impact of the SNR on perpendicular and parallel velocity estimates is however complex to quantify as there is a balance between several effects: on the one hand the least square inversion may favor the accuracy of the parallel velocity but on the other hand high velocities may be less accurately estimated due to short time of flight.

Another limitation of the approach is the positioning of the probe based on real-time M-mode imaging without 2D imaging modality. As it is not a standard procedure for cardiologists, it may require a special training to achieve the positioning. However, M-mode imaging is daily used in cardiology in the parasternal view. Cardiologist can identify easily the RV wall and the septum wall. However, M-mode image requires more time for the positioning and a real-time Bmode imaging would allow a better and faster positioning. Nevertheless, the learning curve was smooth for the cardiologist of the study who was rapidly able to position the transducer without the need of 2D imaging. The entire procedure including positioning and shear wave acquisitions took about 1-2 minutes. A solution to improve the positioning would be to integrate a two-dimensional phased array into the transducer.

V. CONCLUSION

In this study, we introduced a novel approach for non-invasive real-time quantification of transverse isotropic elastic properties. A smart ultrasound device with a small number of transducer elements was developed to measure simultaneously the SWV in three directions and provide the parallel and transverse SWV. We validated the approach using numerical simulations and experiments in calibrated phantoms and ex vivo tissue samples. Finally, we demonstrated the transthoracic feasibility and reproducibility in the human beating heart. The smart ultrasound device has therefore the potential to become a portable and highly disseminable clinical tool for the assessment of myocardial stiffness and function.

REFERENCES

[1] P. Ponikowski *et al.*, '2016 ESC Guidelines for the diagnosis and treatment of acute and chronic heart failure: The Task Force for the diagnosis and treatment of acute and chronic heart failure of the European Society of Cardiology (ESC). Developed with the special contribution of the Heart Failure Association (HFA) of the ESC', *Eur. J. Heart Fail.*, vol. 18, no. 8, pp. 891–975, Aug. 2016, doi: 10.1002/ejhf.592.

[2] 'Myocardial Stiffness in Patients With Heart Failure and a Preserved Ejection Fraction'. https://www.ahajournals.org/doi/epub/10.1161/CIRCULATIONAHA.114.013215 (accessed Oct. 01, 2020).

[3] M. Zile *et al.*, 'Diastolic heart failure--abnormalities in active relaxation and passive stiffness of the left ventricle.', *N. Engl. J. Med.*, 2004, doi: 10.1056/NEJMOA032566.

[4] C. Pislaru *et al.*, 'Ultrasound Strain Imaging of Altered Myocardial Stiffness: Stunned Versus Infarcted Reperfused Myocardium', *Circulation*, vol. 109, pp. 2905–10, Jun. 2004, doi: 10.1161/01.CIR.0000129311.73402.EF.

[5] C. Pislaru *et al.*, 'Myocardial Stiffness by Intrinsic Cardiac Elastography in Patients with Amyloidosis: Comparison with Chamber Stiffness and Global Longitudinal Strain', *J. Am. Soc. Echocardiogr.*, vol. 32, no. 8, pp. 958-968.e4, Aug. 2019, doi: 10.1016/j.echo.2019.04.418.

[6] J.-U. Voigt, 'Direct Stiffness Measurements by Echocardiography', *JACC Cardiovasc. Imaging*, vol. 12, no. 7, pp. 1146–1148, Jul. 2019, doi: 10.1016/j.jcmg.2018.02.004.

[7] A. P. Sarvazyan *et al.*, 'Shear wave elasticity imaging: a new ultrasonic technology of medical diagnostics', *Ultrasound Med. Biol.*, vol. 24, no. 9, pp. 1419–1435, Nov. 1998, doi: 10.1016/s0301-5629(98)00110-0.

[8] J. Bercoff *et al.*, 'Supersonic shear imaging: a new technique for soft tissue elasticity mapping', *IEEE Trans. Ultrason. Ferroelectr. Freq. Control*, vol. 51, no. 4, pp. 396–409, Apr. 2004, doi: 10.1109/tuffc.2004.1295425.

[9] A. Sarvazyan *et al.*, 'Biophysical Bases of Elasticity Imaging', *Acoust Imaging*, vol. 21, Jan. 1995, doi: 10.1007/978-1-4615-1943-0_23.

[10] P. M *et al.*, 'Real-time assessment of myocardial contractility using shear wave imaging.', *J. Am. Coll. Cardiol.*, vol. 58, no. 1, pp. 65–72, Jun. 2011, doi: 10.1016/j.jacc.2011.02.042.

[11] M. Vejdani-Jahromi *et al.*, 'Quantifying Myocardial Contractility Changes Using Ultrasound Based Shear Wave Elastography', *J. Am. Soc. Echocardiogr. Off. Publ. Am. Soc. Echocardiogr.*, vol. 30, no. 1, pp. 90–96, Jan. 2017, doi: 10.1016/j.echo.2016.10.004.

[12] M. Couade *et al.*, 'In vivo quantitative mapping of myocardial stiffening and transmural anisotropy during the cardiac cycle', *IEEE Trans. Med. Imaging*, vol. 30, no. 2, pp. 295–305, Feb. 2011, doi: 10.1109/TMI.2010.2076829.

[13] M. Pernot *et al.*, 'Real-time assessment of myocardial contractility using shear wave imaging.', *J. Am. Coll. Cardiol.*, 2011, doi: 10.1016/j.jacc.2011.02.042.

[14] M. Pernot *et al.*, 'Shear Wave Imaging of Passive Diastolic Myocardial Stiffness', *JACC Cardiovasc. Imaging*, 2016, doi: 10.1016/j.jcmg.2016.01.022.

[15] P. Song *et al.*, 'In vivo transthoracic measurement of end-diastolic left ventricular stiffness with ultrasound shear wave elastography: A pilot study', *2014 IEEE Int. Ultrason. Symp.*, 2014, doi: 10.1109/ULTSYM.2014.0028.

[16] M. Correia *et al.*, 'Ultrafast Harmonic Coherent Compound (UHCC) Imaging for High Frame Rate Echocardiography and Shear-Wave Elastography', *IEEE Trans. Ultrason. Ferroelectr. Freq. Control*, vol. 63, no. 3, pp. 420–431, Mar. 2016, doi: 10.1109/TUFFC.2016.2530408.

[17] O. Villemain *et al.*, 'Myocardial Stiffness Evaluation Using Noninvasive Shear Wave Imaging in Healthy and Hypertrophic Cardiomyopathic Adults', *JACC Cardiovasc. Imaging*, vol. 12, no. 7 Part 1, pp. 1135–1145, Jul. 2019, doi: 10.1016/j.jcmg.2018.02.002.

[18] S. Chatelin *et al.*, 'Modelling the impulse diffraction field of shear waves in transverse isotropic viscoelastic medium', *Phys. Med. Biol.*, vol. 60, no. 9, pp. 3639–3654, May 2015, doi: 10.1088/0031-9155/60/9/3639.

[19] A. Caenen *et al.*, 'Anin silicoframework to analyze the anisotropic shear wave mechanics in cardiac shear wave elastography', *Phys. Med. Biol.*, vol. 63, no. 7, p. 075005, Mar. 2018, doi: 10.1088/1361-6560/aaaffe.

[20] W.-N. Lee *et al.*, 'Mapping myocardial fiber orientation using echocardiography-based shear wave imaging', *IEEE Trans. Med. Imaging*, vol. 31, no. 3, pp. 554–562, Mar. 2012, doi: 10.1109/TMI.2011.2172690.

[21] P. Kohl *et al.*, 'Modelling cardiac mechanical properties in three dimensions', *Philos. Trans. R. Soc. Lond. Ser. Math. Phys. Eng. Sci.*, vol. 359, no. 1783, pp. 1233–1250, Jun. 2001, doi: 10.1098/rsta.2001.0828.

[22] W.-N. Lee *et al.*, 'Ultrasound elastic tensor imaging: comparison with MR diffusion tensor imaging in the myocardium', *Phys. Med. Biol.*, vol. 57, no. 16, pp. 5075–5095, Aug. 2012, doi: 10.1088/0031-9155/57/16/5075.

[23] M. Correia *et al.*, '3D elastic tensor imaging in weakly transversely isotropic soft tissues', *Phys. Med. Biol.*, vol. 63, no. 15, p. 155005, Aug. 2018, doi: 10.1088/1361-6560/aacfaf.

[24] J.-L. Gennisson *et al.*, '4-D ultrafast shear-wave imaging', *IEEE Trans. Ultrason. Ferroelectr. Freq. Control*, 2015, doi: 10.1109/TUFFC.2014.006936.

[25] D. ROYER and E. Dieulesaint, *Elastic Waves in Solids I: Free and Guided Propagation*. Berlin Heidelberg: Springer-Verlag, 2000. Accessed: Sep. 05, 2020. [Online]. Available: https://www.springer.com/gp/book/9783540659327

[26] J. A. Jensen, 'A model for the propagation and scattering of ultrasound in tissue', *J. Acoust. Soc. Am.*, vol. 89, no. 1, pp. 182–190, Jan. 1991, doi: 10.1121/1.400497.

[27] J. A. Jensen and N. B. Svendsen, 'Calculation of pressure fields from arbitrarily shaped, apodized, and excited ultrasound transducers', *IEEE Trans. Ultrason. Ferroelectr. Freq. Control*, vol. 39, no. 2, pp. 262–267, Mar. 1992, doi: 10.1109/58.139123.

[28] V. Vavryčuk, 'On the retrieval of moment tensors from borehole data', *Geophys. Prospect.*, vol. 55, no. 3, pp. 381–391, 2007, doi: 10.1111/j.1365-2478.2007.00624.x.

[29] C. Kasai *et al.*, 'Real-Time Two-Dimensional Blood Flow Imaging Using an Autocorrelation Technique', p. 7.

[30] M. Palmeri *et al.*, 'Quantifying hepatic shear modulus in vivo using acoustic radiation force.', *Ultrasound Med. Biol.*, 2008, doi: 10.1016/j.ultrasmedbio.2007.10.009.

[31] 'Single- and multiple-track-location shear wave and acoustic radiation force impulse imaging: matched comparison of contrast, contrast-to-noise ratio and resolution - PubMed'. https://pubmed.ncbi.nlm.nih.gov/25701531/ (accessed Mar. 29, 2021).

[32] M. Wang *et al.*, 'Imaging Transverse Isotropic Properties of Muscle by Monitoring Acoustic Radiation Force Induced Shear Waves using a 2D Matrix Ultrasound Array', *IEEE Trans. Med. Imaging*, vol. 32, no. 9, pp. 1671–1684, Sep. 2013, doi: 10.1109/TMI.2013.2262948.

[33] F. Tranquart *et al.*, 'Clinical use of ultrasound tissue harmonic imaging', *Ultrasound Med. Biol.*, vol. 25, no. 6, pp. 889–894, Jul. 1999, doi: 10.1016/S0301-5629(99)00060-5.

[34] P. Santos *et al.*, 'Natural Shear Wave Imaging in the Human Heart: Normal Values, Feasibility, and Reproducibility', *IEEE Trans. Ultrason. Ferroelectr. Freq. Control*, vol. 66, no. 3, pp. 442–452, 2019, doi: 10.1109/TUFFC.2018.2881493.

[35] K. F. Kvåle *et al.*, 'Detection of Tissue Fibrosis using Natural Mechanical Wave Velocity Estimation: Feasibility Study', *Ultrasound Med. Biol.*, vol. 46, no. 9, pp. 2481–2492, Sep. 2020, doi: 10.1016/j.ultrasmedbio.2020.04.022.

[36] A. J. Engel *et al.*, 'Cardiac atrial kick shear wave elastography with ultrafast diverging wave imaging: An in vivo pilot study', in *2017 IEEE International Ultrasonics Symposium (IUS)*, Sep. 2017, pp. 1–4. doi: 10.1109/ULTSYM.2017.8092742.

[37] M. Pernot *et al.*, 'ECG-gated, Mechanical and Electromechanical Wave Imaging of Cardiovascular Tissues In Vivo', *Ultrasound Med. Biol.*, vol. 33, no. 7, pp. 1075–1085, Jul. 2007, doi: 10.1016/j.ultrasmedbio.2007.02.003.

[38] A. Petrescu *et al.*, 'Velocities of Naturally Occurring Myocardial Shear Waves Increase With Age and in Cardiac Amyloidosis', *JACC Cardiovasc. Imaging*, vol. 12, no. 12, pp. 2389–2398, Dec. 2019, doi: 10.1016/j.jcmg.2018.11.029.

[39] C. Papadacci *et al.*, '4D Ultrafast Ultrasound Imaging of Naturally Occurring Shear Waves in the Human Heart', *IEEE Trans. Med. Imaging*, vol. 39, no. 12, pp. 4436–4444, Dec. 2020, doi: 10.1109/TMI.2020.3020147.

[40] C. Papadacci *et al.*, '4D simultaneous tissue and blood flow Doppler imaging: revisiting cardiac Doppler index with single heart beat 4D

ultrafast echocardiography', *Phys. Med. Biol.*, vol. 64, no. 8, p. 085013, 10 2019, doi: 10.1088/1361-6560/ab1107.

[41] M. Correia *et al.*, '4D ultrafast ultrasound flow imaging: in vivo quantification of arterial volumetric flow rate in a single heartbeat', *Phys. Med. Biol.*, vol. 61, no. 23, pp. L48–L61, 07 2016, doi: 10.1088/0031-9155/61/23/L48.

[42] S. Salles *et al.*, '3D Myocardial Mechanical Wave Measurements: Toward In Vivo 3D Myocardial Elasticity Mapping', *JACC Cardiovasc. Imaging*, Aug. 2020, doi: 10.1016/j.jcmg.2020.05.037.

[43] A. M. Petrescu *et al.*, 'P2476Non-invasive left ventricular stiffness measurements for assessing diastolic myocardial properties after orthotopic heart transplantation', *Eur. Heart J.*, vol. 40, no. Supplement_1, Oct. 2019, doi: 10.1093/eurheartj/ehz748.0807.